Quantum theory of the mazer. III. Spectrum

Michael Schröder,[1,2] Karl Vogel,[1] Wolfgang P. Schleich,[1,3] Marlan O. Scully,[2,3] and Herbert Walther[3,4]
[1]*Abteilung für Quantenphysik, Universität Ulm, D-89069 Ulm, Germany*
[2]*Department of Physics, Texas A&M University, College Station, Texas 77843*
and Texas Laser Laboratory, Houston Advanced Research Center, The Woodlands, Texas 77381
[3]*Max-Planck-Institut für Quantenoptik, Hans-Kopfermann-Straße 1, D-85748 Garching, Germany*
[4]*Sektion Physik, Ludwig-Maximilians-Universität, München, Germany*
(Received 9 April 1997)

We calculate the spectrum of the micromaser with quantized motion of the pump atoms [M. O. Scully, G. M. Meyer, and H. Walther, Phys. Rev. Lett. **76**, 4144 (1996)] in different velocity regimes. We show that when the kinetic energy of the pump atoms is comparable to the atom-field interaction energy the spectrum of the cavity field is no longer centered at the cavity frequency. In the case of very slow atoms huge broadenings and shifts occur in the vicinity of the mazer resonances. We present approximate analytical results for the spectrum that allow a comparison with the exact numerical calculations. [S1050-2947(97)01611-9]

PACS number(s): 84.40.Ik, 03.65.Nk, 32.80.−t, 42.50.Dv

I. INTRODUCTION

The process of microwave amplification via z-motion–induced emission of radiation, that is, mazer action [1] has opened a new chapter of micromaser physics. In the previous two papers [2,3] of this series—hereafter referred to as paper I and II—we have studied in great detail the statistical properties of the micromaser with quantized center-of-mass motion of the pump atoms. Indeed, paper I presents the general theory of the mazer including the derivation of the master equation and the definition of the various velocity regimes of the pump atoms. Paper II analyzes the mazer for a smooth mode function and suggests a possible experimental realization. In the present paper we focus on the spectrum of the mazer light in the various velocity regimes.

We obtain the spectrum numerically from the eigenvalues and the eigenvectors of the master equation. In particular, we discuss the contributions of the different eigenvalues. For the dominant eigenvalues we are able to derive approximate analytical expressions that we obtain from a perturbation expansion around the mazer resonances [3].

The outline of the paper is as follows. In Sec. II we define the spectrum and calculate it in Sec. III using the eigenvalues and eigenvectors of the master equation. Section IV gives an overview of the spectrum of the micromaser in the different velocity regimes. Throughout the paper we focus on the two analytically tractable mode functions discussed in papers I and II. In Sec. V we present an analytical eigenvalue discussion at the mazer resonances. We conclude in Sec. VI by summarizing our main results.

II. DEFINITION OF THE SPECTRUM

In this section, we define the spectrum of the mazer and introduce an operator $\tilde{\rho}_f$ that satisfies the same equation of motion as the density operator ρ_f of the field. This operator $\tilde{\rho}_f$ allows us to calculate the spectrum.

In accordance with the Wiener-Khintchine theorem [4], we define the steady-state spectrum

$$S(\nu-\nu_c)=\mathrm{Re}\int_0^\infty K(t)e^{-i(\nu-\nu_c)t}dt \tag{1}$$

of the single mode resonator field with creation and annihilation operators $a^\dagger$ and a as the Fourier transform of the two-time correlation function

$$K(t)\equiv\langle a^\dagger(t)a(0)\rangle=\mathrm{Tr}_{f+r}\{a^\dagger(t)a(0)\rho_{f+r}(0)\}. \tag{2}$$

Here ν_c is the cavity frequency and $\rho_{f+r}(0)$ denotes the density operator of the combined field+reservoir $(f+r)$ system. We take the trace over both the field and the reservoir. Moreover, we assume that at $t=0$ we have reached steady state.

With the time evolution operator $U(t)$ for the combined field+reservoir system, the correlation function $K(t)$ reads

$$K(t)=\mathrm{Tr}_{f+r}\{U^\dagger(t)a^\dagger(0)U(t)a(0)\rho_{f+r}(0)\}. \tag{3}$$

Since the field operator $a^\dagger(0)$ acts only on the field we get

$$K(t)=\mathrm{Tr}_f\{a^\dagger(0)\tilde{\rho}_f(t)\}, \tag{4}$$

where we now trace over the field using the moment operator

$$\tilde{\rho}_f(t)\equiv\mathrm{Tr}_r\{U(t)a(0)\rho_{f+r}(0)U^\dagger(t)\} \tag{5}$$

obtained by tracing over the reservoir. With the notation $\tilde{\rho}_n^{(1)}(t)\equiv\langle n|\tilde{\rho}_f(t)|n+1\rangle$ and taking the trace over the field in the photon number representation $|n\rangle$ we find from Eq. (4)

$$K(t)=\sum_n \sqrt{n+1}\,\tilde{\rho}_n^{(1)}(t). \tag{6}$$

In the Markov approximation the moment operator $\tilde{\rho}_f(t)$ satisfies [5] the equation of motion for the field density operator

$$\rho_f(t)\equiv\mathrm{Tr}_r\{U(t)\rho_{f+r}(0)U^\dagger(t)\}, \tag{7}$$

and we therefore obtain $\tilde{\rho}_n^{(1)}(t)$ from the time dependence of the first off-diagonal elements of the field density operator ρ_f. The latter we find from an eigenmode decomposition presented in the following section.

Since $U(t=0)=\mathbf{1}$ the initial condition for $\tilde{\rho}_n^{(1)}(t)$ is

$$\tilde{\rho}_n^{(1)}(0)=\langle n|a(0)\rho_f(0)|n+1\rangle=\sqrt{n+1}P(n+1), \quad (8)$$

where $\rho_f(0)$ and $P(n)=\langle n|\rho_f(0)|n\rangle$ denote the field density operator and the corresponding photon statistics at steady state, respectively.

III. SPECTRUM FROM EIGENMODES OF THE MASTER EQUATION

In this section, we represent the spectrum as a sum of weighted Lorentzians and dispersion curves. The parameters of these curves, such as the widths of the Lorentzians or their weights, follow from the eigenmodes of the master equation.

The master equation, Eq. (29) of paper I of this series, for the density operator ρ_f of the field has the property to couple only elements along the diagonals. By introducing the abbreviation

$$\rho_n^{(1)}\equiv\rho_{n,n+1}\equiv\langle n|\rho_f|n+1\rangle \quad (9)$$

for the nth element of the first off diagonal we can write the equation of motion for $\rho_n^{(1)}$ in the form

$$\dot{\rho}_n^{(1)}=\mathcal{A}_n^{(1)}\rho_{n-1}^{(1)}+\mathcal{B}_n^{(1)}\rho_n^{(1)}+\mathcal{C}_n^{(1)}\rho_{n+1}^{(1)} \quad (10)$$

with the coefficients

$$\mathcal{A}_n^{(1)}\equiv r[R_{b,n}R_{b,n+1}^*+T_{b,n}T_{b,n+1}^*]+Cn_b\sqrt{n(n+1)}, \quad (11)$$

$$\mathcal{B}_n^{(1)}\equiv r[R_{a,n}R_{a,n+1}^*+T_{a,n}T_{a,n+1}^*-1]-C(n_b+1)(n+1/2) -Cn_b(n+3/2), \quad (12)$$

and

$$\mathcal{C}_n^{(1)}\equiv C(n_b+1)\sqrt{(n+1)(n+2)}. \quad (13)$$

We denote the atomic injection rate and the cavity decay constant by r and C, respectively. The number of thermal photons is n_b. Moreover, $R_{a,n}$, $T_{a,n}$, $R_{b,n+1}$, and $T_{b,n+1}$ are the amplitudes of reflection (R) and transmission (T) and simultaneous transition into the lower state (b) or remaining in the upper state (a) of an incident excited atom, respectively. With

$$R_{a,n}\equiv\tfrac{1}{2}(\rho_n^+ +\rho_n^-), \quad T_{a,n}\equiv\tfrac{1}{2}(\tau_n^+ +\tau_n^-) \quad (14)$$

and

$$R_{b,n+1}\equiv\tfrac{1}{2}(\rho_n^+ -\rho_n^-), \quad T_{b,n+1}\equiv\tfrac{1}{2}(\tau_n^+ -\tau_n^-) \quad (15)$$

these amplitudes follow directly [2] from the amplitudes $\tau_n^{\pm}$ and $\rho_n^{\pm}$ of transmission and reflection of the dressed-state components $|\gamma_{n+1}^{\pm}\rangle$. Papers I and II discuss the coefficients $\tau_n^{\pm}$ and $\rho_n^{\pm}$ for two mode functions: the mesa function

$$u(z)\equiv\begin{cases}1 & \text{if } 0\leqslant z\leqslant L\\ 0 & \text{otherwise}\end{cases} \quad (16)$$

describes a mode with sharp edges for a cavity of length L along the motion of the atoms, whereas the sech^2 function

$$u(z)\equiv\mathrm{sech}^2(2z/L)\equiv\frac{1}{\cosh^2(2z/L)} \quad (17)$$

has a smooth behavior. Note that strictly speaking this mode function extends from $-\infty$ to $+\infty$ but due to its exponential decay has an effective range of L. In contrast to paper II, we include in the present paper a factor of 2 in the definition of the sech^2 mode function as to obtain in the Rabi limit the effective coupling strength g, defined in Eq. (1) of paper I.

As outlined in Sec. II the time dependence of ρ_f is identical to that of $\tilde{\rho}_f$. When we combine the elements $\tilde{\rho}_n^{(1)}$ of the first off diagonal of the operator $\tilde{\rho}_f$ to the vector $\mathbf{x}^{(1)}$ with the components

$$[\mathbf{x}^{(1)}(t)]_n\equiv\tilde{\rho}_n^{(1)}(t), \quad (18)$$

the vector $\mathbf{x}^{(1)}$ fulfills the differential equation

$$\dot{\mathbf{x}}^{(1)}(t)=\mathbf{Q}^{(1)}\mathbf{x}^{(1)}(t) \quad (19)$$

with the tridiagonal matrix

$$\mathbf{Q}^{(1)}\equiv\begin{pmatrix}\mathcal{B}_0^{(1)} & \mathcal{C}_0^{(1)} & & \\ \mathcal{A}_1^{(1)} & \mathcal{B}_1^{(1)} & \mathcal{C}_1^{(1)} & \\ & \mathcal{A}_2^{(1)} & \mathcal{B}_2^{(1)} & \ddots \\ & & \ddots & \ddots\end{pmatrix}. \quad (20)$$

The eigenvalues $-\lambda_{\swarrow}^{(1)}$ and eigenvectors $\mathbf{x}_{\swarrow}^{(1)}$ of this matrix follow from the equation

$$\mathbf{Q}^{(1)}\mathbf{x}_{\swarrow}^{(1)}=-\lambda_{\swarrow}^{(1)}\mathbf{x}_{\swarrow}^{(1)} \quad (21)$$

and allow us to write the formal solution

$$\tilde{\rho}_n^{(1)}(t)=\sum_{\swarrow} c_{\swarrow}[\mathbf{x}_{\swarrow}^{(1)}]_n\exp(-\lambda_{\swarrow}^{(1)}t) \quad (22)$$

of the master equation (10). Here the coefficients $c_{\swarrow}$ are determined by the initial condition Eq. (8), that is

$$\sum_{\swarrow} c_{\swarrow}\mathbf{x}_{\swarrow}^{(1)}\equiv\mathbf{x}^{(1)}(0)=(\sqrt{1}P(1),\sqrt{2}P(2),\ldots)^T. \quad (23)$$

When we substitute the formal solution Eq. (22) for $\tilde{\rho}_n^{(1)}(t)$ into the correlation function $K(t)$, Eq. (6), we find

$$K(t)=\sum_{\swarrow} K_{\swarrow}\exp(-\lambda_{\swarrow}^{(1)}t), \quad (24)$$

where we have introduced the weights

$$K_{\swarrow}\equiv c_{\swarrow}\sum_n \sqrt{n+1}[\mathbf{x}_{\swarrow}^{(1)}]_n. \quad (25)$$

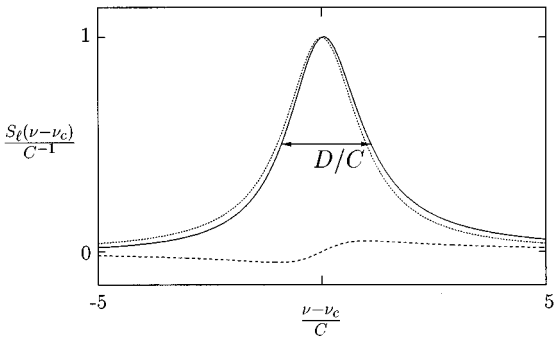

FIG. 1. The contribution $S_\ell(\nu-\nu_c)$ (solid line) of the ℓth eigenvalue to the spectrum $S(\nu-\nu_c)$ is a Lorentzian (dotted line) weighted by $\mathrm{Re}K_\ell$ and a dispersion curve (dashed line) weighted by $\mathrm{Im}K_\ell$. We define the linewidth D/C of the spectrum, which in this case consists of the contribution from a single eigenvalue $\lambda_\ell^{(1)}$, as the full width of $S(\nu-\nu_c)$ at half its maximum. For this picture we have used $\lambda_\ell^{(1)}/C=1$, $\mathrm{Re}K_\ell=1$, and $\mathrm{Im}K_\ell=0.1$.

After performing the Fourier transform of $K(t)$ using the expression Eq. (24) we obtain the spectrum

$$S(\nu-\nu_c)\equiv\sum_\ell S_\ell(\nu-\nu_c)$$

$$=\sum_\ell \mathrm{Re}K_\ell\mathcal{L}(D_\ell,\nu_\ell)+\mathrm{Im}K_\ell\mathcal{D}(D_\ell,\nu_\ell) \tag{26}$$

of the resonator field. Hence each eigenvalue $\lambda_\ell^{(1)}$ contributes a Lorentzian

$$\mathcal{L}(D_\ell,\nu_\ell)\equiv\frac{D_\ell}{D_\ell^2+(\nu-\nu_\ell)^2} \tag{27}$$

centered at $\nu_\ell=\nu_c-\mathrm{Im}\lambda_\ell^{(1)}$ with a full width of $2D_\ell\equiv 2\mathrm{Re}\lambda_\ell^{(1)}$ at half maximum and a dispersion curve

$$\mathcal{D}(D_\ell,\nu_\ell)\equiv\frac{\nu-\nu_\ell}{D_\ell^2+(\nu-\nu_\ell)^2} \tag{28}$$

as demonstrated in Fig. 1.

The integrated contribution

$$\int_{-\infty}^{\infty}S_\ell(\nu-\nu_c)d\nu=\pi\mathrm{Re}K_\ell \tag{29}$$

of S_ℓ is proportional to the weight $\mathrm{Re}K_\ell$, and with the total intensity

$$\int_{-\infty}^{\infty}S(\nu-\nu_c)d\nu=\pi\langle n\rangle \tag{30}$$

of the spectrum following from Eqs. (1) and (2), we get from Eq. (26)

$$\sum_\ell \mathrm{Re}K_\ell=\langle n\rangle. \tag{31}$$

The small perturbation due to the dispersion curve is weighted by $\mathrm{Im}K_\ell$. It does not contribute to the integrated spectrum but shifts some parts of the spectrum to different frequencies, as shown in Fig. 1.

We conclude this section by noting that in general, the matrix $\mathbf{Q}^{(1)}$ is tridiagonal and the eigenvalues and eigenvectors can only be calculated numerically. In the mazer limit, however, we can perform a perturbation expansion around the mazer resonances discussed in papers I and II. This procedure yields simple expressions for $\mathcal{A}_n^{(1)}$, $\mathcal{B}_n^{(1)}$, and $\mathcal{C}_n^{(1)}$, and we obtain a bidiagonal matrix $\mathbf{Q}^{(1)}$. For the latter we can calculate the eigenvalues and eigenvectors analytically. Therefore, we are able to derive approximate analytical expressions for the spectrum, which is the topic of Sec. V.

IV. DISCUSSION OF THE SPECTRUM

As discussed in papers I and II the reflection and transmission coefficients $\rho_n^{\pm}$ and $\tau_n^{\pm}$ can be calculated analytically for two mode functions: the mesa function and the sech^2 function. For these two mode functions we now discuss the micromaser spectrum in the different velocity regimes of the pump atoms: in the Rabi limit, where we have the usual micromaser, in the intermediate regime, and in the mazer limit.

A. Rabi limit

In the limit of very fast atoms with mass M, that is, when their kinetic energy $E\equiv\hbar^2k^2/2M$ is much larger than the atom-field interaction energy $\hbar g\equiv\hbar^2\kappa^2/2M$, all atoms are transmitted. In this limit, that is, for $k/\kappa\gg 1$, the amplitudes $\rho_n^{\pm}$ and $\tau_n^{\pm}$ for both mode functions read $\rho_n^{\pm}=0$ and $\tau_n^{\pm}=\exp(ikL\mp i\sqrt{n+1}g\tau)$ with $g\tau=\kappa^2L/2k$. Here $\tau=LM/\hbar k$ is the interaction time of the atom with the field. Consequently, the master equation of the mazer, Eq. (29) of paper I, reduces to that of the usual micromaser [6] and shows the familiar dynamical and statistical properties. In particular, Ref. [7] has investigated the spectrum of the maser in the Rabi limit.

To bring out the influence of the center-of-mass motion on the spectrum discussed in the next subsections we recall in Figs. 2 and 3 the spectrum $S(\nu-\nu_c)$, the number of photons $\langle n\rangle$, and the linewidth D of the spectrum in their dependence on the pump parameter $\theta=\sqrt{r/C}g\tau$ for $k/\kappa=100$. Here and in the remainder of this paper we define the linewidth of the spectrum as its full width at half its maximum. We note that in the Rabi limit, the characteristics of the micromaser are independent of the mode function and are identical to those of the usual micromaser without quantization of the center-of-mass motion of the pump atoms. The spectrum is always centered at the cavity frequency.

B. Intermediate regime

In the intermediate regime, when the kinetic energy of the atom is comparable to the atom-field interaction energy, that is, when $k/\kappa\approx 1$, the behavior of the micromaser with quantized motion of the pump atoms is different from the usual micromaser. As discussed in paper II, steady-state properties such as the photon number $\langle n\rangle$ are now governed by the

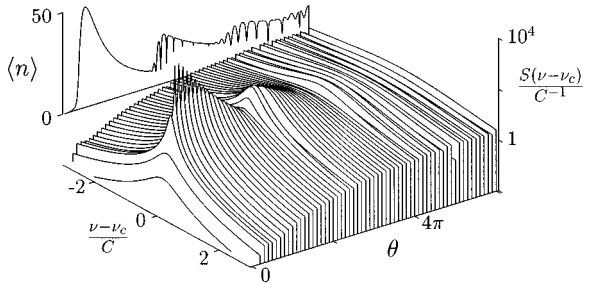

FIG. 2. Spectrum $S(\nu-\nu_c)$ and average photon number $\langle n \rangle$ of the micromaser in the Rabi limit as a function of the pump parameter θ. The spectrum is always symmetric with respect to the cavity frequency ν_c. The trapping states of the micromaser reflect themselves in the spectrum as explained in Ref. [7]. In this limit, neither the quantization of the center-of-mass motion of the atoms nor the detailed shape of the mode function have any influence on the spectrum. The parameters are $k/\kappa=100$, $r/C=50$, and $n_b=10^{-4}$.

parameter kL. We therefore analyze the spectrum in the intermediate regime as a function of this parameter.

In Fig. 4 we show the spectrum $S(\nu-\nu_c)$ and the number of photons $\langle n \rangle$ in their dependence on kL. Here we have used the mesa mode function. We note that the oscillations in the photon number $\langle n \rangle$ translate themselves into oscillations of the width and shift of the spectrum. Moreover, we observe that with increasing parameter kL, the linewidth and the shift increase. To bring this out more clearly we show in Fig. 5 the photon number $\langle n \rangle$, the linewidth D, and the shift $\nu_{\max}-\nu_c$ of the central frequency as a function of kL in the intermediate regime. We indicate the results for the mesa and the sech^2 mode function by solid and dashed lines, respectively. For the sech^2 function, we find that the characteristic oscillations present for the mesa function are less pronounced for $\langle n \rangle$ and are absent in the linewidth and in the shift. The overall behavior, however, is similar. Moreover, whereas $\langle n \rangle$ approaches a constant for large values of kL, the linewidth and the shift continue to increase, as already indicated by Fig. 4. This is due to the fact that the spectrum is governed by the differential equation for the elements of

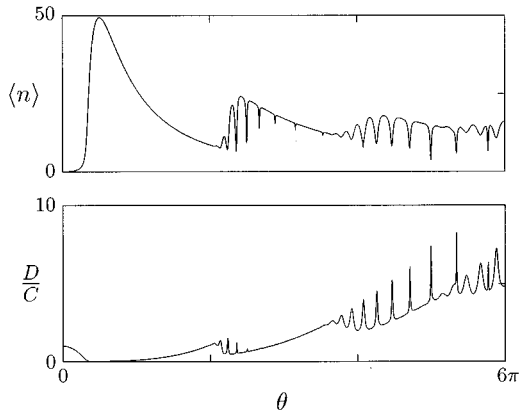

FIG. 3. Average number $\langle n \rangle$ of photons (top) and exact numerical linewidth D of the micromaser spectrum (bottom) in the Rabi limit as a function of the pump parameter θ. The parameters are the same as in Fig. 2.

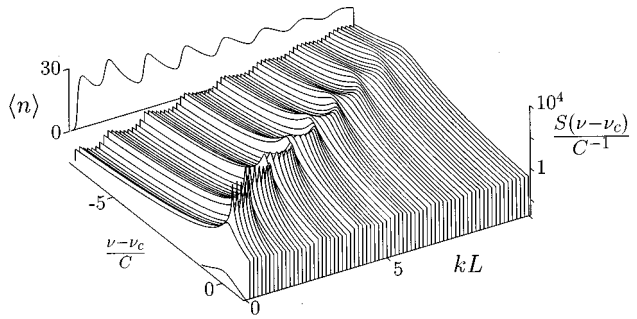

FIG. 4. Spectrum $S(\nu-\nu_c)$ and average photon number $\langle n \rangle$ of the micromaser with quantized motion of the atoms in the intermediate regime in their dependence on the parameter kL. Here we have used the mesa mode function and the parameters are $r/C=50$, $k/\kappa=1$, and $n_b=10^{-4}$.

the first off diagonal rather than the diagonal. The latter determine the photon statistics.

C. Limit of ultracold atoms

In the case of ultracold atoms, that is when $k/\kappa \ll 1$, the behavior of the micromaser changes dramatically. In contrast to the Rabi limit and the intermediate regime, the cavity at steady state contains now in general very few photons. Only under appropriate conditions can the atoms resonantly deposit photons into the resonator. We therefore expect that this different behavior manifests itself also in the spectrum. Moreover, now the spectrum depends sensitively on the mode function. In the following, we therefore discuss the limit of ultracold atoms separately for the mesa and the sech^2 function.

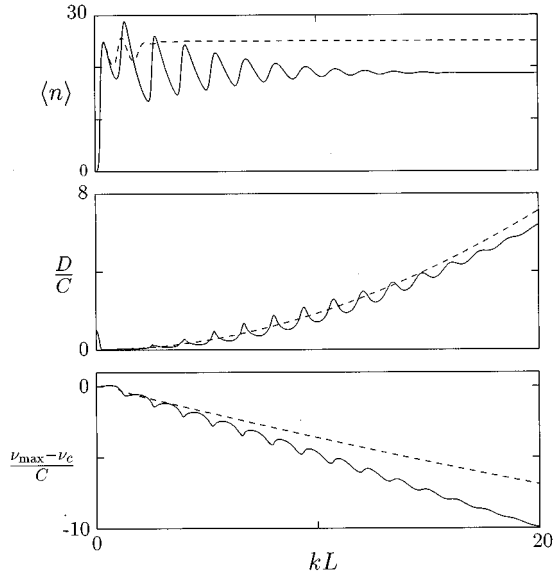

FIG. 5. Average number $\langle n \rangle$ of photons in the micromaser cavity (top), exact numerical linewidth D (middle), and shift $\nu_{\max}-\nu_c$ of the spectrum (bottom) in the intermediate regime as a function of the parameter kL. Solid and dashed lines correspond to the mesa and to the sech^2 mode function, respectively. With increasing kL the linewidth and the shift of the spectrum increase. The parameters are the same as in Fig. 4.

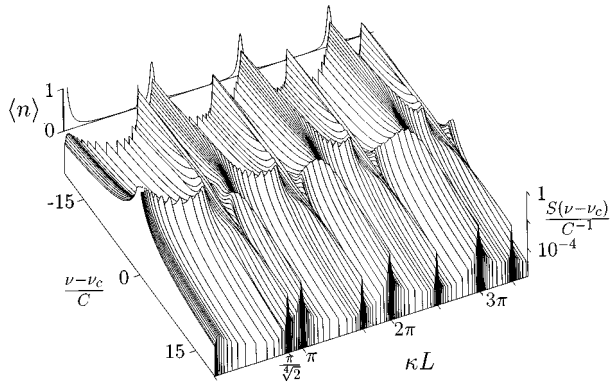

FIG. 6. Spectrum $S(\nu-\nu_c)$ and average photon number $\langle n\rangle$ of the micromaser in the mazer limit using the mesa mode function. At $\kappa L=m\pi/\sqrt[4]{N}$ resonances occur and the linewidth gets large. Before and after the resonances the spectrum gets shifted significantly. The parameters are $r/C=50$, $k/\kappa=0.01$, and $n_b=10^{-4}$.

1. Mesa function

In Fig. 6 we show the micromaser spectrum and the steady-state photon number over a large interval of values of κL. We note a very complex behavior in the vicinity of the resonances [1,2] at

$$\kappa L=\frac{m\pi}{\sqrt[4]{N}}, \tag{32}$$

with N, $m=1,2,\ldots$. To bring this out most clearly we show in Fig. 7 an enlargement of the spectra in the vicinity of the (1,1) and the (2,1) resonances where $\kappa L=\pi$ and $\kappa L=\pi/\sqrt[4]{2}$, respectively. We recall from Sec. VI B of paper I that (N,m) stands for the case of $N-1$ photons initially in the cavity and of m de Broglie half-wavelength fitting in the cavity. Note that in the vicinity of the (2,1) resonance the intensity of the spectrum is significantly smaller than in the

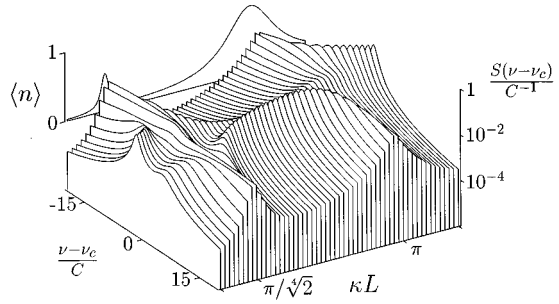

FIG. 7. Spectrum $S(\nu-\nu_c)$ and average photon number $\langle n\rangle$ of the micromaser in the mazer limit in the vicinity of the (1,1) and (2,1) resonances, that is, at $\kappa L=\pi$ and $\kappa L=\pi/\sqrt[4]{2}$, respectively. The behavior at the two resonances is fundamentally different: at the (2,1) resonance the spectrum splits symmetrically into two lines, whereas at the (1,1) resonance the spectrum broadens and shifts as a whole. The integrated spectrum, and hence the average photon number $\langle n\rangle$, is significantly larger at the (1,1) resonance than at the (2,1) resonance. Here we have used the mesa mode function and the same parameters as in Fig. 6.

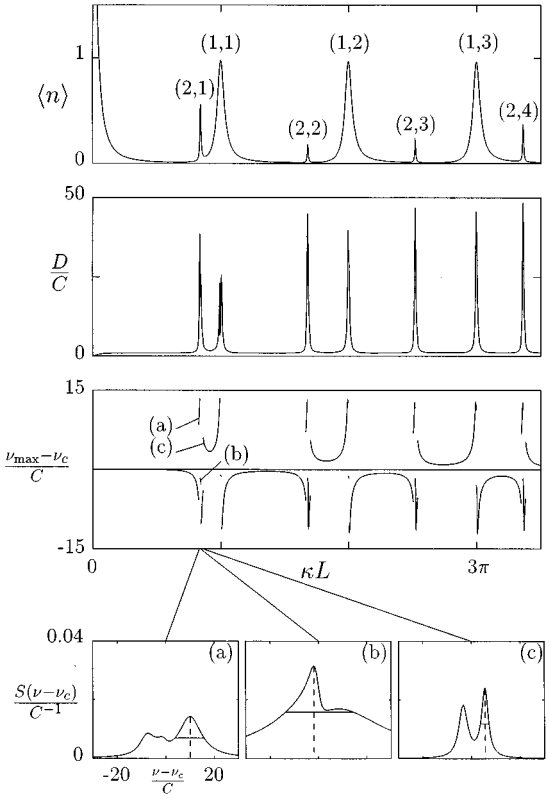

FIG. 8. Average number $\langle n\rangle$ of photons (top), exact numerical linewidth D (middle), and shift $\nu_{\max}-\nu_c$ (bottom) of the micromaser in the mazer limit for the mesa mode function. At resonances, there are huge broadenings of the spectrum. Before and after the resonances, the spectrum gets shifted away from the cavity frequency ν_c. Note that we always plot the full width at half maximum as the linewidth and the shift of the maximum as shift of the spectrum as indicated in the bottom of figure. Here we show the linewidth and the shift of the spectrum at three values of κL by horizontal solid and vertical dashed lines. Due to the complex shape of the spectrum those quantities provide only a rough description and can display sudden jumps as shown by the spectra (a)–(c) in the vicinity of the (2,1) resonance at the bottom of the figure. These examples clearly demonstrate that these definitions of D and $\nu_{\max}$ are problematic for certain cases. Again we have used the same parameters as in Fig. 6.

vicinity of the (1,1) resonance. This is in complete agreement with Fig. 9(b) of paper I and Fig. 8 of the present paper.

This complex behavior of the spectrum also comes out in Fig. 8 where we show the average number $\langle n\rangle$ of photons, the linewidth D, and the shift $\nu_{\max}-\nu_c$ of the maximum of the spectrum from the cavity frequency. At resonant values of κL the linewidth D is significantly broader than the cavity decay rate C. Between the resonances, both are approximately equal. Note that in the case of the $(1,m)$ resonances the width of the resonances in the linewidth D is smaller than the resonances in the steady-state photon number $\langle n\rangle$. However, in the case of the $(2,m)$ resonances they have about the same width. Before and after the resonances, the spectrum experiences a significant shift. Note that before the $(1,m)$ resonances, this shift is towards higher frequencies whereas after the resonances it is towards lower frequencies. In Sec.

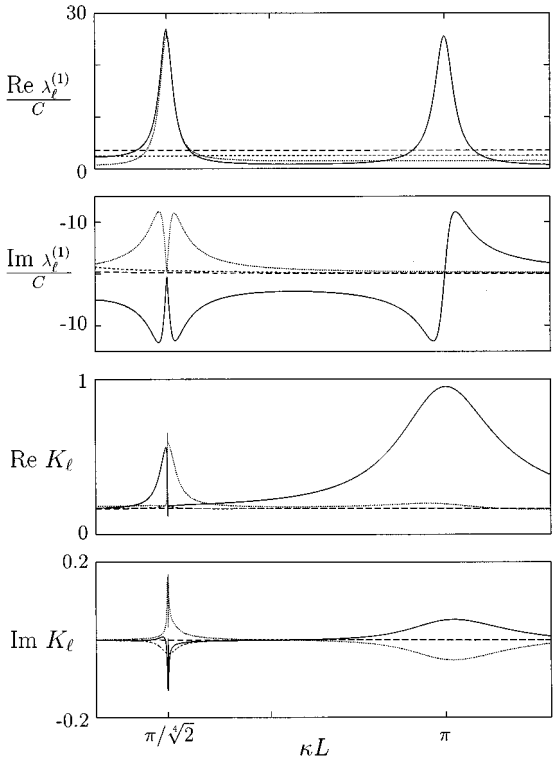

FIG. 9. Four lowest eigenvalues $\lambda_0^{(1)}$, $\lambda_1^{(1)}$, $\lambda_2^{(1)}$, and $\lambda_3^{(1)}$ depicted by solid, dotted, short-, and long-dashed curves, respectively and their weights creating the spectrum shown in Fig. 7 in their dependence on the parameter κL. For each eigenvalue $\lambda_\ell^{(1)}$ we show its real and imaginary part and the weights $\mathrm{Re}K_\ell$ and $\mathrm{Im}K_\ell$. At the (1,1) resonance, that is, at $\kappa L=\pi$, a single eigenvalue dominates the spectrum, whereas at the (2,1) resonance, that is, at $\kappa L=\pi/\sqrt[4]{2}$, an interesting interplay between two eigenvalues occurs. The parameters are the same as in Fig. 6.

V we investigate the behavior in the vicinity of these two resonances in more detail using approximate analytical expressions.

We conclude this subsection by displaying in Fig. 9 the four lowest eigenvalues $\lambda_0^{(1)}$, $\lambda_1^{(1)}$, $\lambda_2^{(1)}$, and $\lambda_3^{(1)}$ and their weights contributing to the spectrum of Fig. 7. Here we use the notation of Eqs. (21) and (22) for the numbering of the eigenvalues. From the behavior of the weights in the vicinity of the (1,1) resonance, we conclude that around $\kappa L=\pi$ the spectrum is dominated by the eigenvalue $\lambda_0^{(1)}$ depicted in Fig. 9 by a solid curve. In contrast, in the vicinity of the (2,1) resonance, that is around $\kappa L=\pi/\sqrt[4]{2}$, an interplay between the eigenvalues $\lambda_0^{(1)}$ and $\lambda_1^{(1)}$, depicted by a dotted curve, determines the spectrum.

2. sech² function

In the case of the smooth sech² mode function the resonance condition [3] reads

$$\kappa L=\frac{2\sqrt{m(m+1)}}{\sqrt[4]{N}}. \tag{33}$$

Note that due to the different definition of the mode function Eq. (17) this resonance condition differs by a factor of two from the resonance condition (C16) of paper II.

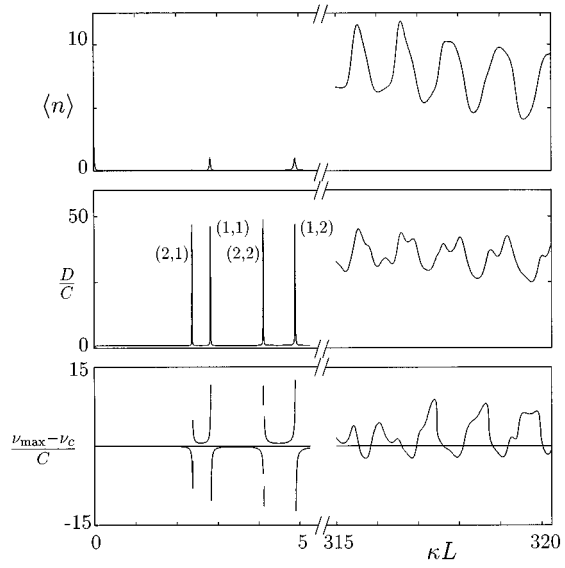

FIG. 10. Average number $\langle n \rangle$ of photons (top), exact numerical linewidth D (middle), and shift $\nu_{\max}-\nu_c$ (bottom) of the micromaser in the mazer limit for the sech² mode function. For small values of κL (left side of the figure), the behavior is similar to that for the mesa function. For large values of κL (right side of the figure), however, the resonances overlap significantly. The parameters are the same as in Fig. 6.

The behavior of the spectrum in the vicinity of these resonances is the same as for the mesa function as long as the resonances do not overlap, that is when $kL \ll 1$. In Fig. 10 we show the average number $\langle n \rangle$ of photons, the linewidth D, and the shift $\nu_{\max}-\nu_c$. For small values of κL, the behavior at the resonances is similar to the case of the mesa function but with different resonant values κL. For large values of κL, however, the resonances overlap significantly and as shown in paper II the emission probability $P_{\mathrm{emission}}(n)$ shows resonances for many values of n. Consequently, there is more than one photon in the resonator at steady state. The shift of the spectrum is less extreme due to the averaging of neighboring resonances and the linewidth D is always significantly larger than the cavity decay rate C.

V. APPROXIMATE ANALYTICAL RESULTS FOR THE SPECTRUM IN THE MAZER LIMIT

In this section, we discuss approximate analytical expressions for the micromaser spectrum in the mazer limit. In particular, we focus on the complex behavior of the spectrum near a resonance as discussed in Sec. IV C. Our treatment heavily makes use of the fact that the width in κL of the resonances in the mazer limit depends on the parameter k/κ. The smaller k/κ, the sharper are the resonances. Indeed, in paper II a perturbation expansion in the vicinity of a general (N,m) resonance has shown that the width is proportional to k/κ. In the present section we prove that the choice of the mode function does not have a significant influence on the statistical properties of the mazer near the $N=1$ and the $N=2$ resonance. In the following, we therefore first present general considerations for the $N=1$ and the $N=2$ resonance, which are followed by the examples of the mesa and the sech² function.

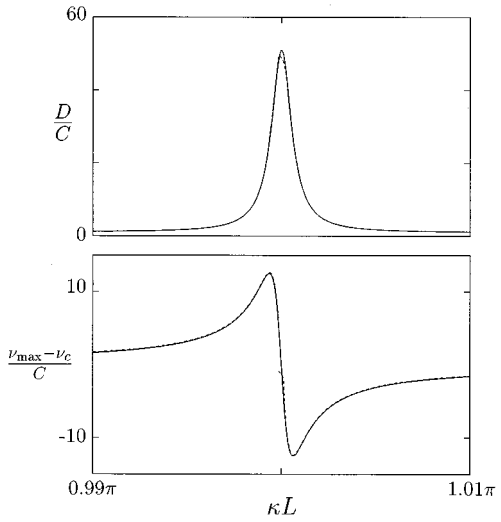

FIG. 11. Analytical results (solid line) for the linewidth D (top) and the shift $\nu_{\max}-\nu_c$ (bottom) from the resonator frequency ν_c in the immediate vicinity of the $\kappa L=\pi$ resonance compared with and contrasted to the exact numerical results (dashed line). Here we have chosen $k/\kappa=0.001$, $r/C=50$, $n_b=0$, and the mesa mode function.

A. $N=1$ resonance

As shown in Appendix A only the eigenvalue

$$\lambda_0^{(1)}\approx\frac{C}{2}+\frac{r}{2}(\rho_0^-+1) \tag{34}$$

contributes to the approximate spectrum

$$S(\nu-\nu_c)=\frac{P(1)\mathrm{Re}\lambda_0^{(1)}}{(\mathrm{Re}\lambda_0^{(1)})^2+(\nu-\nu_c+\mathrm{Im}\lambda_0^{(1)})^2}, \tag{35}$$

where $P(1)$ is given in Eq. (A17). Hence, in the mazer limit and in the neighborhood of the $N=1$ resonance the spectrum is a Lorentzian with a full width at half maximum of

$$\frac{D}{C}=1+\frac{r}{C}(1+\mathrm{Re}\rho_0^-) \tag{36}$$

and with a maximum intensity at the frequency

$$\nu_{\max}-\nu_c=-\frac{r}{2}\mathrm{Im}\rho_0^-. \tag{37}$$

According to this result, the width and the shift of the spectrum are intimately connected with each other via the reflection amplitude ρ_0^-. Therefore, we can specify a Kramers-Kronig relation between the width D and the shift $\nu_{\max}-\nu_c$. This explains the similarity between Fig. 11 and other resonance curves such as the real and imaginary part of the susceptibility.

Furthermore, when we recall the relation Eq. (A18),

$$\langle n\rangle=\frac{r(1+\mathrm{Re}\rho_0^-)}{2C+r(1+\mathrm{Re}\rho_0^-)}, \tag{38}$$

the linewidth takes the form

$$\frac{D}{C}=\frac{1+\langle n\rangle}{1-\langle n\rangle}, \tag{39}$$

which is significantly different from the familiar expression

$$\frac{D}{C}=\frac{\theta^2+1}{4\langle n\rangle} \tag{40}$$

of the Schawlow-Townes linewidth [8,9]. Here we have assumed $n_b=0$ for comparison.

1. Mesa function

According to Appendix A we find for the mesa function the reflection amplitude

$$\rho_0^-=\frac{id/2}{1-id/2} \tag{41}$$

and the expression

$$\frac{\lambda_0^{(1)}}{C}=\frac{1}{2}+\frac{r}{2C}\frac{1+id/2}{1+d^2/4} \tag{42}$$

for the lowest eigenvalue, where

$$d\equiv\left(\kappa L-\frac{m\pi}{\sqrt[4]{N}}\right)\Big/\frac{k}{\kappa} \tag{43}$$

denotes the scaled distance to the resonance Eq. (32) as defined in paper II. With the help of Eq. (38) we therefore arrive at the steady-state photon number

$$\langle n\rangle=\frac{r/2C}{1+r/2C+d^2/4}. \tag{44}$$

According to our analysis the spectrum consists of a single Lorentzian with linewidth

$$\frac{D}{C}=1+\frac{r}{C}\frac{1}{1+d^2/4} \tag{45}$$

and a maximum at

$$\nu_{\max}-\nu_c=-\frac{rd}{4}\frac{1}{1+d^2/4}. \tag{46}$$

Here we have used Eq. (41) for ρ_0^-.

We note the additional term $r/2C$ in the denominator of $\langle n\rangle$, Eq. (44), which is absent in the expressions Eqs. (42) and (45) for the eigenvalue and the linewidth, respectively. It causes the width in κL of the resonance in $\langle n\rangle$ to be larger than the width of the resonance in D by a factor of $\sqrt{1+r/2C}$. Hence the resonance in $\langle n\rangle$ is broader than the resonance in the spectral properties as shown in Fig. 8.

We conclude this subsection by comparing in Fig. 11 these approximate analytical expressions for the linewidth and the shift with the exact numerical curves for $k/\kappa=0.001$. We find excellent agreement. Only on resonance, there is a small deviation due to the second eigenvalue, which is not contained in this approximate analytical description.

2. sech² function

According to Appendix A we find for this mode function

$$\rho_0^- = \frac{id/2}{m+1/2-id/2}, \tag{47}$$

where now

$$d \equiv \left(\kappa L - \frac{2\sqrt{m(m+1)}}{\sqrt[4]{N}} \right) \Big/ \frac{k}{\kappa} \tag{48}$$

denotes the scaled distance to the resonance, Eq. (33). This expression leads via Eq. (36) to the linewidth

$$\frac{D}{C} = 1 + \frac{r}{C} \frac{(m+1/2)^2}{(m+1/2)^2 + d^2/4} \tag{49}$$

and via Eq. (37) to the frequency shift

$$\nu_{\max} - \nu_c = -\frac{rd}{4} \frac{m+1/2}{(m+1/2)^2 + d^2/4}. \tag{50}$$

When we compare Eqs. (41) and (47) for the reflection coefficient ρ_0^-, Eqs. (45) and (49) for the linewidth, and Eqs. (46) and (50) for the shift of the spectrum close to the $N=1$ resonance we find a great similarity. The only difference is an increasing broadening in d with increasing order m. This translates itself via Eqs. (43) and (48) into a broadening in κL, which in turn leads to a smearing out of the resonance for $\kappa L \approx \kappa/k$, as discussed in detail in paper II.

We conclude this subsection by noting that indeed at the $N=1$ resonance the mode function does not play a significant role for the properties of the radiation.

B. $N=2$ resonance

In Appendix B we have shown that close to the $N=2$ resonance and within the framework of our approximations the cavity field in steady state is in the vacuum state. Hence within this approximation the spectrum vanishes, which reflects the fact that the integrated spectrum and hence the average number of photons at the (2,1) resonance is smaller than at the (1,1) resonance as expressed in Fig. 8. In this section we briefly discuss the eigenvalues.

1. Mesa function

According to Appendix B the reflection amplitude

$$\rho_1^- = \frac{id/\sqrt{2}}{1-id/\sqrt{2}} \tag{51}$$

yields the lowest eigenvalues

$$\frac{\lambda_0^{(1)}}{C} = \frac{1}{2} + \frac{r}{2C} \frac{1-id/\sqrt{2}}{1+d^2/2} \tag{52}$$

and

$$\frac{\lambda_1^{(1)}}{C} = \frac{3}{2} + \frac{r}{2C} \frac{1+id/\sqrt{2}}{1+d^2/2}. \tag{53}$$

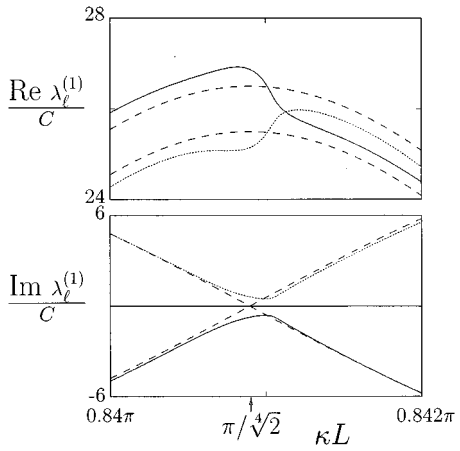

FIG. 12. In the immediate vicinity of the (2,1) resonance at $\kappa L = \pi/\sqrt[4]{2}$ the two eigenvalues $\lambda_0^{(1)}$ and $\lambda_1^{(1)}$ indicated by solid and dotted lines, respectively, interchange their place in the natural sequence of eigenvalues. We compare their exact real (top) and imaginary (bottom) parts with the approximate expressions Eqs. (52) and (53) represented by dashed lines. Here we have used the mesa mode function and the same parameters as in Fig. 6.

They are in good agreement with the numerical results shown in the left part of Fig. 9. The only exception is the close vicinity of the resonance at $\kappa L = \pi/\sqrt[4]{2}$, where the two eigenvalues $\lambda_0^{(1)}$ and $\lambda_1^{(1)}$ swap their position in the sequence of eigenvalues. To bring this out more clearly we compare in Fig. 12 our approximate results for these two eigenvalues with the exact results in the vicinity of $\kappa L = \pi/\sqrt[4]{2}$. We find that the approximate solution describes the principal behavior of both the real and imaginary parts of the eigenvalues very well, with the exception of the very close vicinity of the resonance. Here we observe an avoided crossing of the imaginary parts and an additional crossing of the real parts.

2. sech² function

For the smooth mode function both the numerical and analytical results show no fundamental difference to the case of the mesa function. Indeed according to Appendix B, Eq. (B5) the essential parameter in this case is

$$\rho_1^- = \frac{id/\sqrt{2}}{m+1/2-id/\sqrt{2}}, \tag{54}$$

which, apart from the term $m+1/2$ in the denominator, is identical to the expression Eq. (51) for the mesa function. Hence it is not surprising that this leads to the same results with the additional broadening of the resonances with increasing orders m.

VI. CONCLUSION

We have discussed the spectrum of the mazer in the different velocity regimes, that is, in the Rabi limit, in the intermediate regime, and in the mazer limit. In particular, we have found a broadening and a shift of the spectrum near the mazer resonances. To get a shift, the strict mazer limit is not necessary. Indeed, already when the kinetic energy is of the

order of the energy of the vacuum dressed states, the spectrum gets shifted significantly. In the mazer regime the broadening and the shift are most pronounced. Moreover, our approximate analytical treatment shows an interesting connection between the linewidth and the frequency shift of the spectrum provided by the complex amplitude of the reflected matter wave, that is of the pump atoms. In this way the center-of-mass motion of the atoms manifests itself in the spectrum of the quantized electromagnetic field in the resonator.

ACKNOWLEDGMENTS

We thank Fam Le Kien, M. Löffler, G. M. Meyer, and M. S. Zubairy for fruitful discussions. This work was partially supported by the DFG. M.O.S. wishes to thank the ONR, the Welch Foundation, and TARP for their support. M.S. is grateful to the Studienstiftung des deutschen Volkes. W.P.S. and H.W. acknowledge financial support from the European Commission through the TMR Research Training Network ''Microlasers and Cavity QED.''

APPENDIX A: SPECTRUM NEAR $N=1$ RESONANCE

In this Appendix, we derive approximate analytical expressions for the eigenvalues, the zeroth eigenvector, and the mazer spectrum in the neighborhood of the $N=1$ resonance. The present treatment is valid for both mode functions and in the absence of thermal photons, that is, $n_b=0$.

For $N=1$ we find from the resonance conditions Eqs. (C14) and (C20) of paper II the resonance photon number $n_{\rm res}=0,15,80,255,\ldots$ and $n_{\rm res}=0,3,8,24,\ldots$ for the mesa and the sech^2 function, respectively. In general, there are so few photons in the resonator that we can neglect the higher photon numbers. In this case for both the mesa function and the sech^2 function the amplitudes of reflection and transmission for the $N=1$ type resonance take the form

$$\rho_n^+=-1,\ \rho_n^-=\begin{cases}\rho_0^- & \text{if } n=0\\ -1 & \text{otherwise}\end{cases} \tag{A1}$$

and

$$\tau_n^+=0,\ \ \tau_n^-=\begin{cases}\tau_0^- & \text{if } n=0\\ 0 & \text{otherwise.}\end{cases} \tag{A2}$$

Here only the coefficients ρ_0^- and τ_0^- depend on the form of the mode function. In the case of the mesa function Eq. (C11) of paper II yields

$$\rho_0^-=\frac{id/2}{1-id/2} \tag{A3}$$

and

$$\tau_0^-=\frac{(-1)^m}{1-id/2}, \tag{A4}$$

whereas for the sech^2 mode Eqs. (C18) and (C19) of paper II provide us with

$$\rho_0^-=\frac{id/2}{m+1/2-id/2} \tag{A5}$$

and

$$\tau_0^-=\frac{(-1)^m(m+1/2)}{m+1/2-id/2}. \tag{A6}$$

Since our definition of the mode function, Eq. (17), differs from the one used in paper II, Eq. (7), by a factor of two in the argument of the sech function, we have substituted in these results $d/2$ for d.

We now use the expressions Eqs. (A1) and (A2) for $\rho_n^\pm$ and $\tau_n^\pm$ to calculate the amplitudes $R_{a,n}$, $T_{a,n}$, $R_{b,n+1}$, and $T_{b,n+1}$ from Eqs. (14) and (15) and find from Eqs. (11)–(13) the quantities

$$\mathcal{A}_n^{(1)}=0, \tag{A7}$$

$$\mathcal{B}_n^{(1)}=\begin{cases}-\dfrac{C}{2}-\dfrac{r}{2}(\rho_0^-+1) & \text{if } n=0,\\ -C\left(n+\dfrac{1}{2}\right) & \text{otherwise,}\end{cases} \tag{A8}$$

and

$$\mathcal{C}_n^{(1)}=C\sqrt{(n+1)(n+2)}, \tag{A9}$$

where we have assumed $n_b=0$. Therefore the matrix

$$\mathbf{Q}^{(1)}=\begin{pmatrix}\mathcal{B}_0^{(1)} & \mathcal{C}_0^{(1)} & & \\ 0 & \mathcal{B}_1^{(1)} & \mathcal{C}_1^{(1)} & \\ & 0 & \mathcal{B}_2^{(1)} & \ddots\\ & & \ddots & \ddots\end{pmatrix}, \tag{A10}$$

defined by Eq. (20), is bidiagonal and we can read the eigenvalues

$$\lambda_0^{(1)}=-\mathcal{B}_0^{(1)}=\frac{C}{2}+\frac{r}{2}(\rho_0^-+1) \tag{A11}$$

and

$$\lambda_\ell^{(1)}=-\mathcal{B}_\ell^{(1)}=C\left(\ell+\frac{1}{2}\right) \tag{A12}$$

with $\ell=1,2,3,\ldots$ directly from the diagonal.

We now calculate the expansion coefficients c_ℓ according to Eq. (23). We therefore have to first derive the steady-state photon statistics

$$P(n)=P(0)\left(\frac{r}{C}\right)^n\prod_{m=1}^{n}\frac{P_{\rm emission}(m-1)}{m} \tag{A13}$$

using the emission probability

$$P_{\rm emission}(n)=\frac{1}{4}(|\rho_n^+-\rho_n^-|^2+|\tau_n^+-\tau_n^-|^2) \tag{A14}$$

as shown in paper I. When we substitute Eqs. (A1) and (A2) into Eq. (A14) we find

$$P_{\text{emission}}(n)=\begin{cases}(1+\text{Re}\rho_0^-)/2 & \text{if } n=0\\ 0 & \text{otherwise.}\end{cases} \tag{A15}$$

Here we have used the constraint

$$|\rho_0^-|^2+|\tau_0^-|^2=1 \tag{A16}$$

for particle conservation.

Hence from Eq. (A13) we arrive at the steady-state photon statistics

$$P(n)=\begin{cases}\dfrac{2C}{2C+r(1+\text{Re}\rho_0^-)}, & n=0,\\ \dfrac{r(1+\text{Re}\rho_0^-)}{2C+r(1+\text{Re}\rho_0^-)}, & n=1,\\ 0, & n=2,3,\ldots\end{cases} \tag{A17}$$

with the steady-state photon number

$$\langle n\rangle=\frac{r(1+\text{Re}\rho_0^-)}{2C+r(1+\text{Re}\rho_0^-)}. \tag{A18}$$

Note that according to this equation $\langle n\rangle$ is always smaller than unity. This is consistent with our starting approximation of neglecting the higher photon numbers in n_{res}.

With the help of Eq. (A17) the initial condition Eq. (23) reduces to

$$\sum_{\ell=0}^{\infty} c_\ell \mathbf{x}_\ell^{(1)}=(\sqrt{1}P(1),0,0,\ldots)^T. \tag{A19}$$

The zeroth eigenvector

$$\mathbf{x}_0^{(1)}=(1,0,0,\ldots)^T \tag{A20}$$

immediately yields

$$c_\ell=K_\ell^{(1)}=\delta_{\ell,0}P(1). \tag{A21}$$

Therefore, only the eigenvalue $\lambda_0^{(1)}$ contributes to the spectrum and we find according to Eqs. (26)–(28)

$$S(\nu-\nu_c)=\frac{P(1)\text{Re}\lambda_0^{(1)}}{(\text{Re}\lambda_0^{(1)})^2+(\nu-\nu_c+\text{Im}\lambda_0^{(1)})^2}, \tag{A22}$$

that is, a Lorentzian with a full width at half maximum of

$$\frac{D}{C}=\frac{2\text{Re}\lambda_0^{(1)}}{C}=1+\frac{r}{C}(1+\text{Re}\rho_0^-). \tag{A23}$$

The maximum of the spectrum Eq. (A22) lies at the frequency

$$\nu_{\max}-\nu_c=-\text{Im}\lambda_0^{(1)}=-\frac{r}{2}\text{Im}\rho_0^-. \tag{A24}$$

In Sec. V we compare these approximate analytical results with the exact numerical treatment.

APPENDIX B: SPECTRUM NEAR $N=2$ RESONANCE

In this Appendix, we perform an analysis analogous to Appendix A and derive approximate analytical expressions for the eigenvalues and the spectrum in the mazer limit. We now focus on the $N=2$ resonance.

We recall from Eqs. (C14) and (C20) of paper II the values $n_{\text{res}}=1,31,161,511,\ldots$ and $n_{\text{res}}=1,7,17,49,\ldots$ of the resonance photon numbers corresponding to the mesa and the sech^2 function, respectively. Again neglecting higher photon numbers, the general $N=2$ resonance gives rise to the amplitudes

$$\rho_n^+=-1,\ \rho_n^-=\begin{cases}\rho_1^- & \text{if } n=1\\ -1 & \text{otherwise}\end{cases} \tag{B1}$$

of reflection and the amplitudes

$$\tau_n^+=0,\ \tau_n^-=\begin{cases}\tau_1^- & \text{if } n=1\\ 0 & \text{otherwise}\end{cases} \tag{B2}$$

of transmission. These results are valid for both mode functions. For the mesa function we find from Eq. (C11) of paper II the explicit expressions

$$\rho_1^-=\frac{id/\sqrt{2}}{1-id/\sqrt{2}} \tag{B3}$$

and

$$\tau_1^-=\frac{(-1)^m}{1-id/\sqrt{2}}, \tag{B4}$$

whereas Eqs. (C18) and (C19) of paper II predict

$$\rho_1^-=\frac{id/\sqrt{2}}{m+1/2-id/\sqrt{2}} \tag{B5}$$

and

$$\tau_1^-=\frac{(-1)^m(m+1/2)}{m+1/2-id/\sqrt{2}} \tag{B6}$$

for the case of the sech^2 potential. Again as in Appendix A we have substituted $d/2$ for d in the expressions of paper II.

Following the example of Appendix A the results for $\rho_n^\pm$ and $\tau_n^\pm$, Eqs. (B1) and (B2), lead to

$$\mathcal{A}_n^{(1)}=0, \tag{B7}$$

$$\mathcal{B}_n^{(1)}=\begin{cases}-\dfrac{C}{2}-\dfrac{r}{2}[(\rho_1^-)^*+1], & \text{if } n=0\\ -\dfrac{3C}{2}-\dfrac{r}{2}(\rho_1^-+1), & \text{if } n=1\\ -C\left(n+\dfrac{1}{2}\right) & \text{otherwise,}\end{cases} \tag{B8}$$

and

$$\mathcal{C}_n^{(1)}=C\sqrt{(n+1)(n+2)}, \tag{B9}$$

where again we have assumed $n_b=0$. As for the $N=1$ resonance in Appendix A, the matrix

$$\mathbf{Q}^{(1)}=\begin{pmatrix}\mathcal{B}_0^{(1)} & \mathcal{C}_0^{(1)} & & \\ 0 & \mathcal{B}_1^{(1)} & \mathcal{C}_1^{(1)} & \\ & 0 & \mathcal{B}_2^{(1)} & \ddots \\ & & \ddots & \ddots\end{pmatrix}, \tag{B10}$$

defined by Eq. (20), is again bidiagonal. Hence the two lowest eigenvalues read

$$\lambda_0^{(1)}=-\mathcal{B}_0^{(1)}=\frac{C}{2}+\frac{r}{2}[(\rho_1^-)^*+1] \tag{B11}$$

and

$$\lambda_1^{(1)}=-\mathcal{B}_1^{(1)}=\frac{3C}{2}+\frac{r}{2}(\rho_1^-+1). \tag{B12}$$

The higher eigenvalues follow from

$$\lambda_\ell^{(1)}=-\mathcal{B}_\ell^{(1)}=C\left(\ell+\frac{1}{2}\right), \tag{B13}$$

where $\ell=2,3,4,\ldots$.

To derive the expansion coefficients c_ℓ from Eq. (23) we first calculate the emission probability $P_{\text{emission}}(n)$, Eq. (A14), using the expressions Eqs. (B1) and (B2) for $\rho_n^{\pm}$ and $\tau_n^{\pm}$. After minor algebra we arrive at

$$P_{\text{emission}}(n)=\begin{cases}(1+\text{Re}\rho_1^-)/2 & \text{if } n=1\\ 0 & \text{otherwise,}\end{cases} \tag{B14}$$

where we have used the condition

$$|\rho_1^-|^2+|\tau_1^-|^2=1 \tag{B15}$$

for particle conservation. Due to $P_{\text{emission}}(0)=0$ the steady-state photon statistics reduces for $n_b=0$ to

$$P(n)=\begin{cases}1, & n=0\\ 0, & n\geqslant 1,\end{cases} \tag{B16}$$

that is, to the photon statistics of the vacuum.

Hence we find from the condition Eq. (23), that is, from $\Sigma_{\ell=0}^{\infty}c_\ell\mathbf{x}_\ell^{(1)}=0$, the coefficients

$$c_\ell\equiv 0 \tag{B17}$$

and the resulting spectrum is

$$S(\nu-\nu_c)\equiv 0. \tag{B18}$$

This is consistent with Eq. (30) when we recall that due to Eq. (B16) we have $\langle n\rangle=0$.

[1] M. O. Scully, G. M. Meyer, and H. Walther, Phys. Rev. Lett. **76**, 4144 (1996).

[2] G. M. Meyer, M. O. Scully, and H. Walther, paper I, Phys. Rev. A **56**, 4142 (1997).

[3] M. Löffler, G. M. Meyer, M. Schröder, M. O. Scully, and H. Walther, paper II, Phys. Rev. A **56**, 4153 (1997).

[4] N. Wiener, Acta Math. **55**, 117 (1930); A. Y. Khintchine, Math. Ann. **109**, 604 (1934).

[5] C. W. Gardiner, *Handbook of Stochastic Methods* (Springer, Berlin, 1990).

[6] P. Filipowicz, J. Javanainen, and P. Meystre, Phys. Rev. A **34**, 3077 (1986); L. A. Lugiato, M. O. Scully, and H. Walther, *ibid.* **36**, 740 (1987).

[7] M. O. Scully, H. Walther, G. S. Agarwal, Tran Quang, and W. P. Schleich, Phys. Rev. A **44**, 5992 (1991); Trang Quang, G. S. Agarwal, J. Bergou, M. O. Scully, H. Walther, K. Vogel, and W. P. Schleich, *ibid.* **48**, 803 (1993); K. Vogel, W. P. Schleich, M. O. Scully, and H. Walther, *ibid.* **48**, 813 (1993); W. C. Schieve, and R. R. McGowan, *ibid.* **48**, 2315 (1993); Ning Lu, Opt. Commun. **103**, 315 (1993); for a discussion of the spectrum at trapping states, see S. Qamar and M. S. Zubairy, Phys. Rev. A **44**, 7804 (1991); Ning Lu, *ibid.* **47**, 1347 (1993); Phys. Rev. Lett. **70**, 912 (1993).

[8] M. O. Scully and W. E. Lamb, Jr., Phys. Rev. **159**, 208 (1967).

[9] M. Sargent, M. O. Scully, and W. E. Lamb, *Laser Physics* (Addison-Wesley, Reading, MA, 1974).